Advances in Engineering Research : Possibilities and Challenges
ISSN Print: 3079-5192
ISSN Online: 3079-5206
https://doi.org/10.63313/AERpc.9051

Grating structures are fabricated inside glass based on femtosecond laser parallel processing technology

Yaofei Ma[1,2]. Shufeng Sun[1,2,*]. Jin Wang[1,2*]. Fengyun Zhang[1,2]. Xuecheng Gao[1,2]. Tao Wei[1,2]. Zhihao Qu[1,2] and Pingping Wang[1,2]
[1]Discipline Innovation and Wisdom Introduction Base of High-end Laser Intelligent Manufacturing Technology and Equipment, school of Mechanical and Automotive Engineering, Qingdao University of Technology, Qingdao 266520, China
[2]Key Laboratory of High-end Laser Manufacturing Technology and Equipment of Shandong Province, school of Mechanical and Auto-motive Engineering, Qingdao University of Technology, Qingdao 266520, China
Email: sunshufeng@qut.edu.cn

How to cite this paper: Ma, Y. F., Sun, S. F., Wang, J., Zhang, F. Y., Gao, X. C., Wei, T., Qu, Z. H., & Wang, P. P. (2025). Grating structures are fabricated inside glass based on femtosecond laser parallel processing technology. Advances in Engineering Research: Possibilities and Challenges, 2(2), 81-90. ISSN Print: 3079-5192; ISSN Online: 3079-5206.
https://doi.org/10.63313/AERpc.9051
Published: 2025-09-02

Abstract

Femtosecond laser single-focus scanning has the problem of low efficiency when manufacturing large-area structures. This paper proposes a multi-focus parallel processing method based on the weighted Gerchberg-Saxton (GS) algorithm. A multi-focus hologram was designed and loaded onto a spatial light modulator to achieve uniform energy distribution. The effects of repetition frequency, processing times and scanning speed on the morphology of microchannels were systematically studied, and the uniformity was all above 90%. Using the optimized process parameters, a grating structure with a cross-sectional width of approximately 29.315 μm was fabricated inside the glass by the three-focal parallel process. Compared with single-focus scanning, this method triples the efficiency while maintaining high quality, providing a promising path for the manufacturing of scalable photonic devices.

Keywords

Femtosecond laser; Spatial light modulator; holography; Glass gratings

1. Introduction

Femtosecond lasers have revolutionized micro–nano fabrication owing to their unique combination of ultrashort pulse duration, extremely high peak power, and minimized thermal damage [1, 2]. Through nonlinear absorption, they enable precise structural modification inside transparent materials without surface ablation [3, 4], which has opened new opportunities in micro-optics, integrated photonics, and microfluidics [3, 5]. Over the past decade, femtosecond laser direct writing has been extensively used for the fabrication of waveguides, diffractive optical elements, and microfluidic channels [6]. However, the conventional single-focus scanning strategy remains inherently inefficient for large-area structures, often requiring prolonged exposure that compromises uniformity and increases process variability [7].

To overcome the throughput bottleneck, holographic parallel processing based on spatial light modulators (SLM) has emerged as a powerful approach [8]. By designing computer-generated holograms (CGH), an incident beam can be flexibly shaped into a multi-focus array, enabling simultaneous machining at multiple sites [9]. This capability not only increases fabrication speed but also provides programmable control over the spatial distribution of foci. In recent years, several studies have validated the promise of this strategy. Wang et al. demonstrated the fabrication of multilayer three-dimensional structures in glass using fractional Fourier transform combined with SLMs [10]. Yao et al. introduced dynamic multifocus laser sculpturing (DMLS), which allowed freeform three-dimensional structures in glass to be directly processed with high fidelity [11]. More recently, holographic multifocus two-photon polymerization has been employed for 3D nanoprinting, producing over 400 uniform foci and achieving ultrahigh throughput of 1.49×10^8 voxels/s while preserving nanoscale resolution [12]. These advances highlight the potential of holographic beam shaping for efficient, flexible, and high-resolution fabrication.

Nevertheless, several challenges remain unresolved. First, maintaining uniform energy distribution among multiple foci is difficult, often leading to variations in processing quality across an array [13]. Second, most complex structures reported to date still require auxiliary steps such as chemical etching or post-polishing, limiting the directness and practicality of internal fabrication. Third, despite notable demonstrations, systematic investigations into how processing parameters—such as repetition frequency, scanning speed, and the number of passes—influence both morphology and uniformity remain scarce. Meanwhile, fundamental studies on femtosecond laser–material interactions have revealed promising pathways: extended filamentation inside glass enables long-range energy delivery [14], and high-aspect-ratio nanochannels have been achieved using Bessel beams, reaching diameters of ~2 μm and depths exceeding 80 μm [15]. While these works broaden the processing toolkit, they do not directly address the central issue of simultaneously achieving high throughput, high uniformity, and high precision for large-area internal structuring.

In this work, we propose a femtosecond laser multi-focus parallel processing method based on a weighted Gerchberg–Saxton (GS) algorithm. The iterative weighting ensures balanced energy distribution and high diffraction efficiency, enabling stable multi-focus holograms on the SLM. We systematically study the effects of repetition frequency, scanning speed, and processing times on microchannel morphology, achieving over 90% uniformity among three channels. Under optimized conditions, glass gratings with ~29.4 μm line width are fabricated, showing good consistency. Compared with single-focus scanning, our method improves efficiency by ~3× while maintaining optical-grade quality and eliminating the need for post-processing.

2. Material and method

2.1. Material

The material used is ultra-thin float glass, which features high light transmittance, good heat resistance and strong chemical stability. It is widely applied in the construction industry, electronic equipment, photovoltaic industry and medical industry, etc. Its thickness is 1 mm and the area is 50×50mm2. The main components include SiO2 (72%), CaO (13.5%), and Na2O + K2O (8.1%).

2.2. Method

We established an optical path system, as shown in **Figure 1.** The spot diameter of the laser beam emitted was 3 mm, which was expanded to 12 mm through the beam expansion system. The effective window area of the spatial light modulator is 16× 12.8mm ^{2}, which can be fully utilized. Under the conditions of an input laser center wavelength of 1035 nm, a pulse width pw of 300 fs, and a maximum single-pulse energy pe of 50 μJ, the maximum peak power density of the laser is approximately 0.3 GW/cm^2. The peak power density threshold that the spatial light modulator can withstand is 5.4 GW/cm^2. The maximum average power density of the laser is approximately 35.4 W/cm^2, while the highest tested average power density of the spatial light modulator is 32.7 W/cm^2. Therefore, the spatial light modulator cannot meet the requirements of full-power processing. In addition, due to the relatively low damage threshold of optical components in the optical path system, after comprehensive consideration, we set the laser power range from 0 to 4 W. The laser power is measured by a laser power meter of the brand COHERENT and model FieldMaxII-TOP.

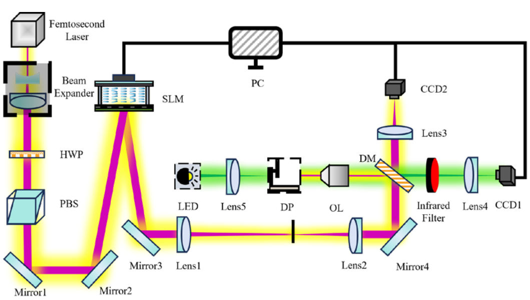

Figure 1. Optical Path System.

In the experiment, we adopted the weighted Gerchberg-Saxton (GS) algorithm to design the multi-focus array hologram. The algorithm flow chart is shown in **Figure 2**. Take the generation of a 1×3 focal array hologram as an example. The pixel size of the spatial light modulator is 1272×1024 pixels. To integrate all the information and enhance the computational efficiency of the holographic algorithm, we set the hologram to 1280×1280 pixels and then cropped it to 1272×1024 pixels through a program. Since the light modulated by the spatial light modulator generates zero-order light, we set the three focus positions at deviations from the center position, namely (550,600), (600,600), and (650,600), with an X-axis interval of 50 pixels and a Y-axis offset of 40 pixels. Set the number of iterations of the two algorithms to 50 times.

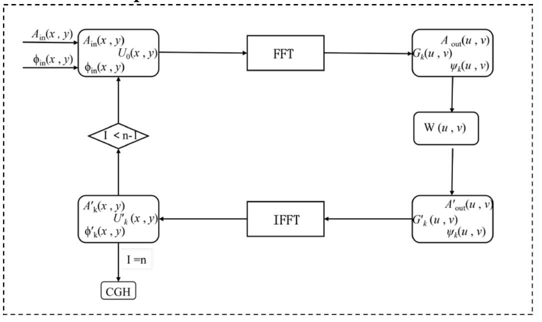

Figure 2. Flowchart of the GS algorithm.

3. Results and Discussion.

3.1. The Influence of Repetition Frequency on Parallel Processing

Laser repetition frequency, defined as the number of pulses per unit time, strongly influences power, energy delivery, and processing quality. At constant pulse energy, higher frequency increases average power but reduces energy per pulse. Thus, selecting an appropriate repetition frequency is essential to improve energy utilization, avoid over-ablation, and ensure processing quality. Here, we first examine its effect on femtosecond laser processing.

In the experiment, we set the initial parameters of the laser as follows: the laser power was set to 1.7W, the scanning speed was set to 0.1mm /s, the processing times were set to once, and the control single factor variable was the repetition frequency. The experimental results are shown in **Figure 3**, and they were measured and analyzed using a laser confocal microscope. **Figures 3 (a)** and **(b)** show the topography of a single channel processed by three-focus machining at different repetition frequencies, where **Figure 3 (a)** is an enlarged view of **Figure 3 (b)**. We selected the repetition frequencies of 800 kHz, 400 kHz, 200 kHz, 100 kHz, 80 kHz, 50 kHz, 40 kHz, 20 kHz, 10 kHz and 8 kHz for research because the pulse frequency division coefficient of the laser is an integer ranging from 1 to 255. **Figure 3 (c)** shows the contour maps of the measurement and analysis results at different repetition frequencies. When the repetition frequency is 800 kHz, the depth of the microchannel reaches the maximum value of 3.014 μm. When the average power output by the laser remains unchanged, as the laser repetition frequency decreases, the size of the single channel also shows a gradually decreasing trend. This is because the reduction in repetition frequency leads to a decrease in the number of laser pulses per unit time, while the average power of the laser remains unchanged, resulting in a decrease in the energy of a single laser pulse and a gradual weakening of energy deposition when interacting with the material.

To reduce randomness, we repeated the experiment three times and obtained consistent results, confirming their reliability. The red-marked values may stem from platform vibration. At low repetition frequencies, the ablation threshold of ultra-thin float glass is high, leading to weak processing effects. Thus, increasing repetition frequency effectively improves microstructure processing efficiency.

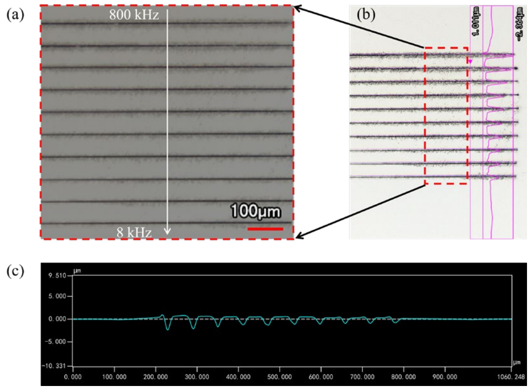

Figure 3. Schematic diagram of processing with different repetition frequencies.

3.2. The influence of processing times on parallel processing

In this study, we set the laser parameters as a laser power of 3.4 W, a pulse repetition frequency of 800 kHz, and a scanning speed of 0.1 mm/s. We set the output power of the femtosecond laser to 0.32W to verify the modulation effect of beam splitting, and then increased the power for processing.

We selected processing times of 1, 2, 3, 4, 5, 6, 7, 8, 9, and 10 respectively to study the characteristics of microchannels. **Figure 4 (a)** shows the morphology of microchannels with different scan counts. The experimental results show that when the processing times are once, the width and depth of the microchannels are the lowest, which are 5.032 μm and 0.558 μm respectively. As the number of processing times increases, the width and depth of microchannels will gradually increase **(Figures 4 (b)** and **(c))** . When the processing times are more than 9 times, the width of the microchannel will reach a level similar to the size of the laser focused spot. At this time, the width will not increase significantly but tend to be flat, gradually reaching the maximum value, which can be as high as 6.112 μm. Meanwhile, as the number of processing times increases, the laser energy will constantly interact with the material around the focus, thereby leading to an increase in the depth of the microchannel.

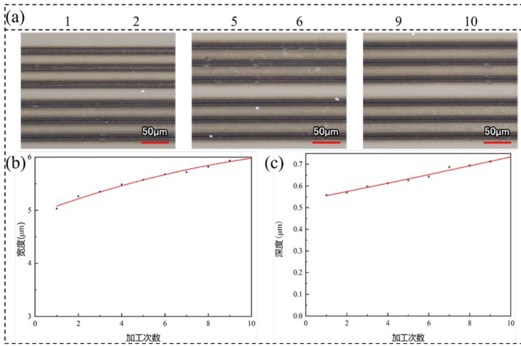

Figure 4. Microchannel morphology and width and depth curves for different machining times (a) Morphology of three-focused microchannels with different number of machining; (b) Plot of microchannel width vs. number of machining; (c) Plot of microchannel depth vs. number of Machining.

To assess the uniformity of the three foci generated by the weighted GS algorithm, three microchannels were measured, each with three datasets averaged. Multiple cross-sectional measurements verified that the algorithm ensures high processing uniformity. However, as shown in **Figure 5**. The microchannels are distributed parallel on their surfaces, with uniform spacing between adjacent channels. However, there are obvious ablation marks in the black areas on their surfaces. By observing **Figure 5**, it can be found that there is a distinct etching line at the center of each microchannel. The black edge part is not a microchannel structure but a mixture of ablation residue and molten material. These black parts are usually caused by the fact that during the laser processing, when the high-energy laser beam irradiates the material surface, it triggers the thermal decomposition and vaporization of the substance, generating gas and solid residues that deposit after cooling.

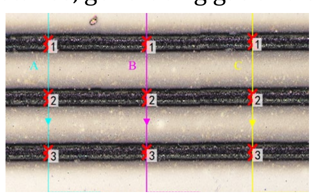

Figure 5. Observation diagram of the experimental method.

In the experiment, we randomly selected the experimental data when the processing times were 1, 4, and 8 times respectively for characterization and analysis. Mark each group of microchannels as A, B and C. For each group of microchannels, we conducted three data collections, that is, we selected three groups of data from A, B and C respectively for measurement. The method of taking the average of multiple measurements aims to enhance the reliability and accuracy of the data. Taking the processing times of 4 as an example, within the allowable error range, the experimental data are shown in **Table 1**.

Table 1. Microchannel Width Data Sheet.

	1	2	3
A	5.466μm	5.295μm	5.419μm
B	5.854μm	5.187μm	5.611μm
C	5.522μm	5.228μm	5.703μm
Average value	5.614μm	5.210μm	5.578μm

In the table, the average width of the microchannel was obtained by averaging three sets of data (5.466 μm, 5.854 μm, 5.522 μm), and the calculation result was 5.614 μm. The homogeneity of microchannels is evaluated by taking the ratio of the minimum to the maximum value in the average. Based on the data (5.614 μm, 5.210 μm, 5.578 μm), the calculated homogeneity was 92.8%. Based on the same calculation process, the other two sets of data were analyzed, and the results in **Table 2** were obtained.

Table 2. Data table of microchannel widths for different processing times.

	1	2	3	Uniformity
Once	5.312μm	5.398μm	5.998μm	93.2%
Twice	5.614μm	5.210μm	5.578μm	92.8%
Three times	6.061μm	6.481μm	6.059μm	93.5%
Average value	5.662μm	5.696μm	5.878μm	96.3%

It can be seen from the experimental data in **Table 2** that the increase in the number of processing times leads to an increase in the average width of the microchannel. As the number of processing times increases, the interaction between laser energy and the material intensifies, and the etching degree of the material gradually deepens, thereby leading to an increase in the average width of microchannels. However, the uniformity of the widths of the three microchannels shows a stable trend, with a uniformity of over 90%, and is not significantly affected by the number of processing times.

3.3. The influence of processing speed on parallel processing

To verify the influence of speed on the microchannel, the experimental parameter was set to the average laser power of 3.4W, the laser pulse repetition frequency is 800 kHz, at 0.01mm /s, 0.03mm /s, 0.05mm /s, 0.07mm/s, 0.09mm /s, 0.1mm /s, 0.12mm /s, 0.15mm /s, 0.18mm /s. Experiments were conducted at fourteen processing speeds of 0.2mm /s, 0.22mm/s, 0.25mm /s, 0.28mm /s, and 0.3mm /s. Due to the small size of the materials used and the limitations of the clamping device and the moving platform, it is not advisable to adopt a larger processing speed during the processing. The result is shown in **Figure 6**. When the processing speed is 0.01 mm/s, the width and depth values of the microchannel are the highest, being 5.498 μm, and 0.582 μm, respectively. Compared with the number of processing times, the processing speed has a relatively small influence on the microchannel. As the processing speed increases, the total energy of the laser energy acting on the surface of the microchannel per unit time will decrease. The width and depth of microchannels show a decreasing trend. This is because the laser energy is distributed in a narrower area. Even if the laser energy density remains constant, an increase in processing speed will reduce the time the laser acts per unit length, thereby reducing the depth to which the material is removed. The depth may tend to stabilize but increase slightly. Because the increase in processing speed reduces the time that the laser acts on the material surface, but at the same time, it will cause the laser focused spot to spread somewhat, which may result in a slight increase in depth. And the width tends to decrease.

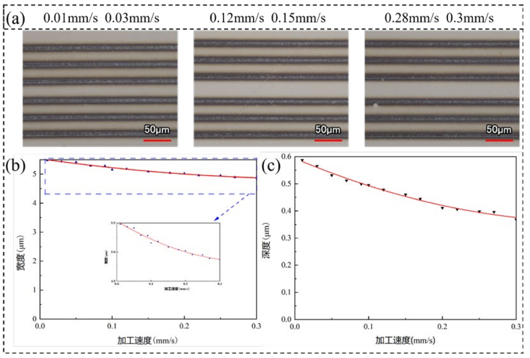

Figure 6. Microchannel morphology and width and depth curves at different machining speeds (a) Microchannel machining topography at different machining speeds; (b) Microchannel width vs. machining speed; (c) Microchannel depth vs. machining speed.

We randomly selected the experimental data with processing speeds of 0.03mm/s, 0.1mm/s and 0.25mm/s to evaluate the uniformity of the microchannel width. Within the rotational speed range of 0.01mm/s to 0.3mm/s, the uniformity curve fluctuates relatively little. This indicates that as the processing speed increases, the interaction between the laser and the material weakens, resulting in a decrease in the etching degree of the microchannels. Although the processing speed has increased and the trend of microchannel width variation has become more stable, the uniformity still remains above 90%. This indicates that the weighted GS algorithm has better stability and uniformity at different processing speeds.

3.4. Multi-focus parallel processing: Processing grating structures inside glass

Through previous experiments, we have established the experimental foundation for multi-focus parallel processing, including focus stability and laser parameter Settings. In this chapter, we set the laser power to 3.4 W, the pulse repetition frequency to 800 kHz, the pulse width to 300 fs, and the scanning speed to 0.1 mm/s. First, perform an ultrasonic water bath cleaning on the glass to remove impurities adhering to its surface. Then fix the glass onto the three-axis precision moving platform. Use the COMS1 camera to image and observe the approximate position of the focus on the glass surface, and precisely locate the focus by setting it to move a certain distance. Move the Z-axis upward by 0.4mm to focus the focal point on the interior of the glass. Next, through the program setting, the laser moves from the 9mm position on the X-axis to the 45mm position at a speed of 0.1mm /s, then moves 0.15mm upward along the Y-axis at a speed of 0.03mm /s, and then returns the laser from the 45mm position to the 9mm position. And move it upward again along the Y-axis by 0.15mm. The above steps constitute one processing procedure, and this process is repeated. **Figure 7 (a)** shows a schematic diagram of the processing of a three-focus parallel grating, and **Figure 7 (b)** shows a physical image of the laser focused into the interior of the glass for processing.

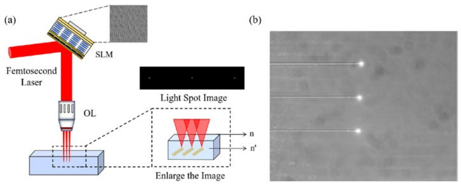

Figure 7. Parallel processing of gratings by three-focused femtosecond laser (a) Schematic diagram of three-focused parallel processing of internal glass gratings; (b) Physical diagram of three-focused parallel processing of internal glass gratings.

In the experiment, we set the internal triple focal interval to 60 pixels, and the actual interval was approximately 30 μm. Firstly, explore the relationship between the pixel spacing of the hologram design focus and the actual processing focus spacing to achieve precise control over the focus distribution. After measurement and analysis, it was found that the ratio of the designed pixel pitch of the hologram to the actual processing focal pitch was approximately 2:1. Then, we fabricated a 30× 35mm grating inside the glass in a single processing by using the three-focal parallel processing method. As shown in **Figure 8**, the processing inside the glass hardly changes the transparency of the glass, and the grating successfully displays the colored stripe pattern under the light.

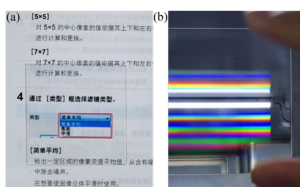

Figure 8. Gratings for parallel processing with three focus femtosecond lasers (a) Schematic diagram of grating transmittance; (b) Effect of grating.

4. Conclusion

In this study, a spatial light modulator was used to modulate femtosecond laser into a multifocus, and a grating was fabricated inside the glass through parallel processing. The experiment first explored the influence of repetition frequency, processing times and processing speed on parallel processing. The method of etching microchannels was adopted for the experiment, and the optimal process parameters were obtained: processing speed 0.1 mm/s, processing times 1, laser pulse repetition frequency 800 kHz, and average power 3.4 W. The uniformity of the multi-focus parallel processing beam was characterized based on the microchannel width and the roughness of the processing channel lines. The results showed that the uniformity was always above 90%, verifying the feasibility of the weighted GS algorithm modulation for generating multi-focus parallel processing.

Acknowledgements

This work was supported by Qingdao University of Technology, Discipline Innovation and Wisdom Introduction Discipline lnnovation and Wisdom Introduction Base of High-end Laser Intelligent Manufacturing Technology and Equipment

References

[1] Sugioka K, Cheng Y. Ultrafast lasers—reliable tools for advanced materials processing[J]. Light: Science & Applications, 2014, 3(4): e149-e149.

[2] Guo B, Sun J, Hua Y, et al. Femtosecond laser micro/nano-manufacturing: theories, measurements, methods, and applications[J]. Nanomanufacturing and Metrology, 2020, 3(1): 26-67.

[3] Yang L, Wei J, Ma Z, et al. The fabrication of micro/nano structures by laser machining[J]. Nanomaterials, 2019, 9(12): 1789.

[4] Shin S, Hur J G, Park J K, et al. Thermal damage free material processing using femtosecond laser pulses for fabricating fine metal masks: Influences of laser fluence and pulse repetition rate on processing quality[J]. Optics & Laser Technology, 2021, 134: 106618.

[5] He F, Liao Y, Lin J, et al. Femtosecond laser fabrication of monolithically integrated microfluidic sensors in glass[J]. Sensors, 2014, 14(10): 19402-19440.

[6] Sugioka K, Cheng Y. Femtosecond laser three-dimensional micro-and nanofabrication[J]. Applied physics reviews, 2014, 1(4).

[7] Sun H, Li J, Liu M, et al. A review of effects of femtosecond laser parameters on metal surface properties[J]. Coatings, 2022, 12(10): 1596.

[8] Zhang H, Hasegawa S, Toyoda H, et al. Three-dimensional holographic parallel focusing with feedback control for femtosecond laser processing[J]. Optics and Lasers in Engineering, 2022, 151: 106884.

[9] Kuang Z, Liu D, Perrie W, et al. Fast parallel diffractive multi-beam femtosecond laser surface micro-structuring[J]. Applied Surface Science, 2009, 255(13-14): 6582-6588.

[10] Wang J, Hayasaki Y, Zhang F, et al. Three-dimensional holographic femtosecond laser parallel processing method with the fractional Fourier transform for glass substrates[J]. Ceramics International, 2022, 48(11): 16364-16373.

[11] Reese Z C, Fox J C, Taylor J, et al. Evolution of cooling length in parts created through laser powder bed fusion additive manufacturing[C]//Proceedings— 2018 ASPE and euspen Summer Topical Meeting: Advancing Precision in Additive Manufacturing. 2018: 183-188.

[12] Zhang L, Wang C, Zhang C, et al. High-throughput two-photon 3D printing enabled by holographic multi-foci high-speed scanning[J]. Nano Letters, 2024, 24(8): 2671-2679.

[13] Qu Z, Jiang H, Wang K, et al. Deep-learning-aided multi-focal hologram generation[J]. Optics & Laser Technology, 2025, 182: 112056.

[14] Yan T, Ji L. Ultrafast laser filamentation in transparent solids[J]. Ultrafast Science, 2023, 3: 0023.

[15] Bhuyan M K, Courvoisier F, Lacourt P A, et al. High aspect ratio nanochannel machining using single shot femtosecond Bessel beams[J]. Applied Physics Letters, 2010, 97(8).